

Special Issue

Characterization of agitation environments in 250 ml spinner vessel, 3 L, and 20 L reactor vessels used for animal cell microcarrier culture

Raghavan V. Venkat & Jeffrey J. Chalmers

Department of Chemical Engineering, The Ohio State University, Columbus, OH 43210–1180, USA

Key words: 3-D PTV, bioreactor agitation, flow structures, scale-up

Abstract

Three dimensional particle tracking velocimetry (3-D PTV) was used to characterize the flow fields in the impeller region of three microcarrier reactor vessels. Three typical cell culture bioreactors were chosen: 250 ml small-scale spinner vessels, 3 L bench-scale reactor, and 20 L medium-scale reactor. Conditions studied correspond to the actual operating conditions in industrial setting and were determined based on the current scale-up paradigm: the Kolmogorov eddy length criterion. In this paper we present characterization of hydrodynamics on the basis of flow structures produced because of agitation. Flow structures were determined from 3-D mean velocity results obtained using 3-D PTV. Although the impellers used in 3 L and 20 L reactors were almost identical, the flow structures produced in the two reactors differed considerably. Results indicate that near geometric scale up does not necessarily amount to scale-up of flow patterns and indicates that intensity as well as distribution of energy may vary considerably during such a scale-up.

Background

Microcarrier cultures are traditionally grown in stirred reactor systems. These reactors exhibit two areas believed responsible for cell damage due to hydrodynamics: the forces associated with gas bubbles used for aeration and the turbulent forces generated in the impeller region of agitated vessels (Papoutsakis, 1991). Although microcarrier culture is widely used in small scale (sub 20 L) operation, success at large scale is limited (Cherry and Papoutsakis, 1990; Aunins *et al.*, 1993). Several researchers (Croughan *et al.*, 1987, Cherry and Papoutsakis, 1986, etc.) have concentrated on understanding the effects of agitation in microcarrier cultures; but few efforts have been made to mechanistically understand impeller agitation and *flow structures* produced by the impeller and other internals. There are also no studies that have been performed to relate flow structures with possible damage in shear sensitive cultures (Aunins *et al.*, 1993).

Most of the past research on agitation in stirred vessels, not just in animal cell culture, but in the area of

mixing, has recommended the use of global parameters as scaleup criteria (Smith *et al.*, 1990). Examples of these global parameters are: impeller tip speeds, impeller Reynolds Number, pumping efficiency, power per unit volume (PV^{-1}), and more recently the Kolmogorov eddy length. These global parameters do not account for 'local' non-homogeneity of flow in mixing vessels. Non-homogeneity in flow is the result of structures that are produced by the impeller and other internals within the vessel. Associated with these structures are high levels of hydrodynamic energy (Stoots and Calabrese, 1995). These local flow structures are a complex function of geometry and operating conditions of the vessels and cannot be described adequately by global scale-up parameters.

Global parameters are popular because they are reasonably easy to determine and apply/work adequately in most circumstances. In the past it was difficult and time consuming to characterize flow structures that exist in mixing vessels. However, recent advances in computer technology and image processing (Adrian, 1991) is allowing flow visualization techniques such

as: 3-D particle tracking velocimetry (3-D PTV), scanning particle image velocimetry (SPIV), and 2-D PIV to be performed easily and rapidly. These flow visualization techniques allow complex flow structures to be determined. Consequently, instead of using global parameters to characterize flow in mixing vessels, it is becoming possible to develop 'local' energy characterizations of flow within vessels.

We propose that the difficulty in scale-up of micro-carrier culture is the result of the lack of preservation of local flow structures as the reactor vessels are scaled-up. Implicit in this hypothesis is the concept (shown by Stoots and Calabrese, 1995) that highly localized regions of high energy dissipation exist and that these areas are associated with flow structures. It is also suggested that cell damage on microcarriers takes place in these regions of energy dissipation above a threshold level. Finally, it is suggested that as a system is scaled-up, preservation of minimum levels of energy dissipation is desired to provide sufficient mixing and prevent clumping while preventing the maximum level of energy dissipation from exceeding the threshold level which causes damage.

In previous publications (Venkat *et al.*, 1993; Venkat *et al.*, 1996), the flow structure and associated energy dissipation in a 250 ml spinner flask were presented. In this paper the flow structure in three 'typical' bioreactors is presented: the 250 ml spinner studied in the previous publication, a 3 L bench-scale bioreactor, and a model of a 20 L pilot-scale bioreactor. The studies were conducted under conditions of constant Kolmogorov eddy length (Table 1) one of the 'global' parameters suggested to be used for scale-up. Furthermore, these vessels are routinely operated in an industrial setting under these same conditions. Publications in preparation compare and discuss the various energy dissipation rates associated with the flow structures within these different vessels. Finally, to test the hypothesis that a threshold level of energy dissipation is needed to damage/remove cells from microcarriers, experimental studies in well-defined hydrodynamic conditions are being conducted.

Materials and methods

Bioreactors and details of the impeller geometry

Figure 1 shows schematic of the three reactor vessels used in our study. The 250 ml spinner vessel was a Corning vessel (cat. No. 26502-250, Sigma Chemi-

Table 1. 3-D PTV experimental conditions. Also includes the Kolmogorov eddy length values calculated based on the methodology suggested by Cherry and Papoutsakis (1986)

Reactor	Impeller Diameter (cm)	Impeller agitation (RPM)	Impeller Reynolds Number	Kolmogorov eddy length (microns) ^a
Spinner ^b	5.6	90	6.7×10^3	98
		150	1.1×10^4	71
		210	1.6×10^4	58
3 L Holtz ^c	8.4	45	7.6×10^4	98
		60	1.0×10^4	78
		75	1.3×10^4	66
20 L ^c	15.6	45	2.6×10^4	71
		72	4.2×10^4	50

^a – Kolmogorov eddy length calculations were based on the impeller volume.

^b – Spinner paddle power number calculated as suggested by Aunins *et al.*, 1989.

^c – Power number calculations are approximations based on the assumption that the impeller is similar to a four-blade axial impeller classified by Oldshue as a A2 type (Oldshue, 1983).

cal Co., St. Louis, MO) and details of the impeller geometry have been described previously (Venkat *et al.*, 1996). The 3 L bioreactor was a Holtz Bioengineering reactor (presently) Wheaton Instruments, NJ, and the 20 L reactor a round-bottom Pyrex glass vessel modeled after the Bioengineering 20 L animal cell bioreactor. The impellers used in the 3 L and 20 L vessels were almost identical and operated in an up-pumping mode. The impeller used was a three-bladed 45 ° inclined impeller. Though widely used, there is no information on the flow structures generated by this impeller.

Flow markers

Two flow markers were used in our experiments: Polystyrene microcarriers and Amberlite ion exchange particles. Polystyrene microcarriers ranging in diameter from 150 to 212 μm (Cat. P102-1521, SoloHill Labs Inc., Ann Arbor, MI) were used in the spinner vessel experiments. Due to visualization limitations Amberlite particles (Cat. No. 15622, Poly Sciences Inc., Warrington, PA) of 300–500 μm diameter were used in the 3 L and 20 L experiments. Both the particles had a density of 1.02 g/cc and were dyed to improve visualization. Particle loading of 1 g/l, 0.3 g/l, and 0.025 g/l were used for the spinner, 3 L and 20 L experiments, respectively.

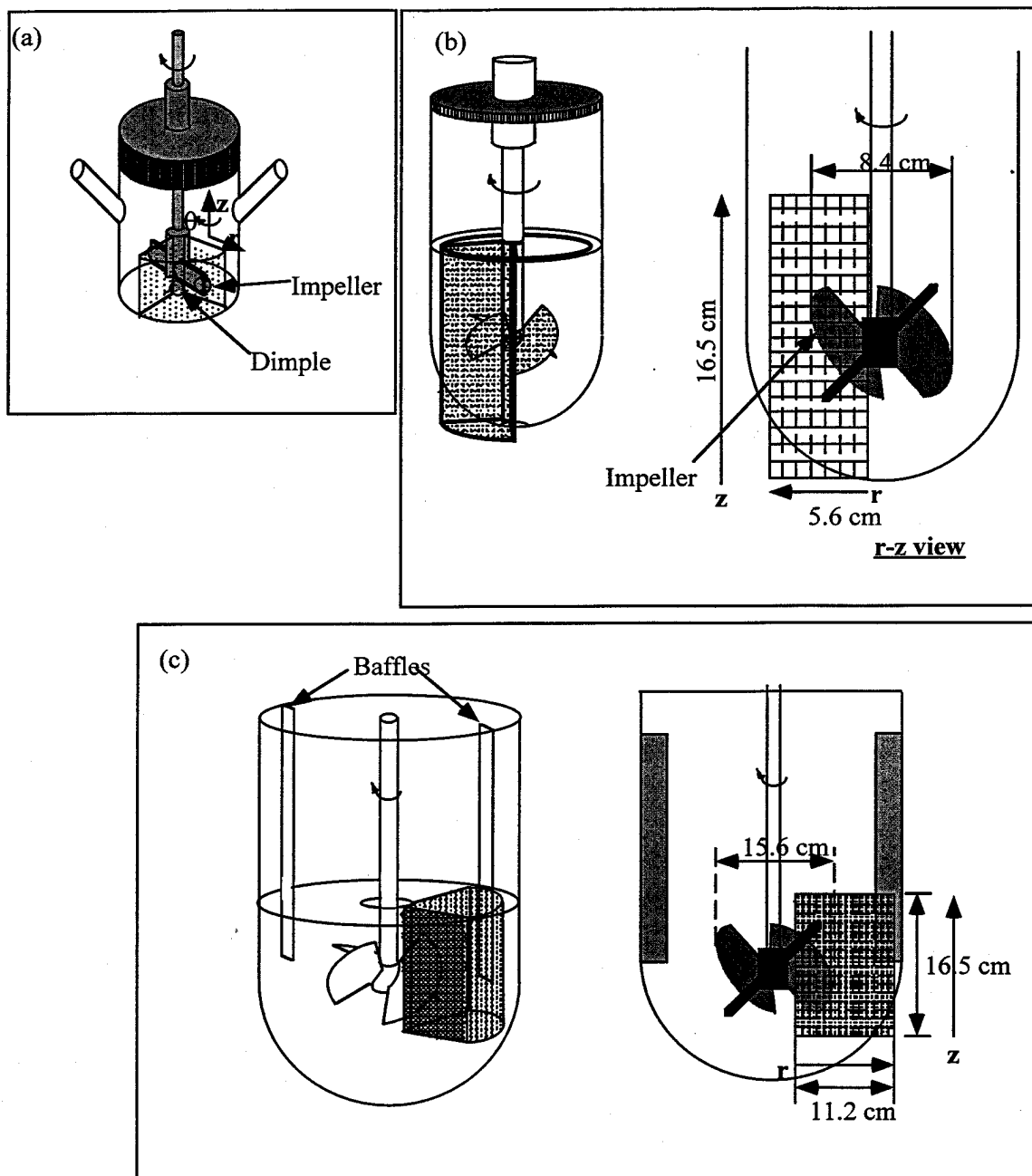


Figure 1. (a) Flow volume and 3-D perspective of the 250 ml spinner flask. (b) Flow volume and 3-D perspective of the 3 L bench-scale Holtz bioreactor. (c) Flow volume and 3-D perspective of the 20 L baffled bioreactor. Shaded region shows the field of view.

Stereo-visualization equipment and 3-D PTV

Stereo visualization arrangement and the details of the 3-D PTV have been explained previously and the origi-

nal publication (Guezennec *et al.*, 1994) describes PTV algorithm in detail. The apparatus used for the spinner experiments has been described earlier by (Venkat *et al.*, 1996). For the 3 L and 20 L experiments a Cohu

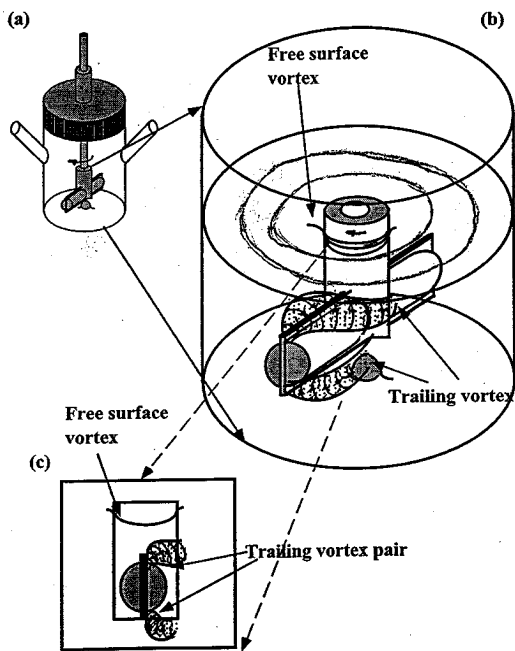


Figure 2. Schematic of impeller flow in the spinner vessel. (a) Schematic of the spinner vessel. (b) Magnified view of the impeller stream and the free surface. Figure shows the pair of trailing vortices coming off the impeller tip and free surface vortex formed around the shaft at the agitation rate of 210 rpm. (c) Front view of the impeller tip showing the trailing vortex and the free surface vortex (Reprinted from Venkat *et al.*, 1996).

CCD4915 video camera (Cohu Inc., San Diego, CA) equipped with a Canon zoom lens (28–105 mm) and macro attachment, was used. The lens was shuttered at 2000 s^{-1} and the experiment recording using a Panasonic AG-7355 SVHS Video cassette recorder.

Ensemble averaging

A statistically stationary turbulent flow has no dependence on time. Therefore, to obtain mean flow information, one simply has to take the time average (Tennekes and Lumley, 1972). However, flow field in the impeller stream is periodic in nature and is a function of time or position of the impeller. Therefore, to obtain mean flow quantities, the experiment must be repeated multiple times, the impeller positions of each experiment matches, and the data combined from each individual experiment. Another reason for ensemble averaging was because the instantaneous data density resulting from 3-D PTV was not high enough for interpolation of velocities onto a meaningful three dimensional reg-

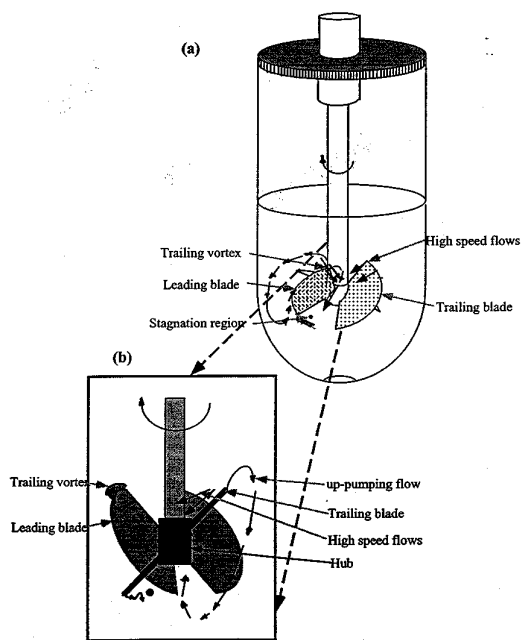


Figure 3. Schematic of the impeller flow in the case of the 3 L bench-scale reactor operated at 60 rpm (a) Impeller stream and overall circulation induced by the agitator. Figure shows the small trailing vortex coming off the tip of the impeller blade. (b) Magnified view (almost side view) of the impeller stream shown in (a).

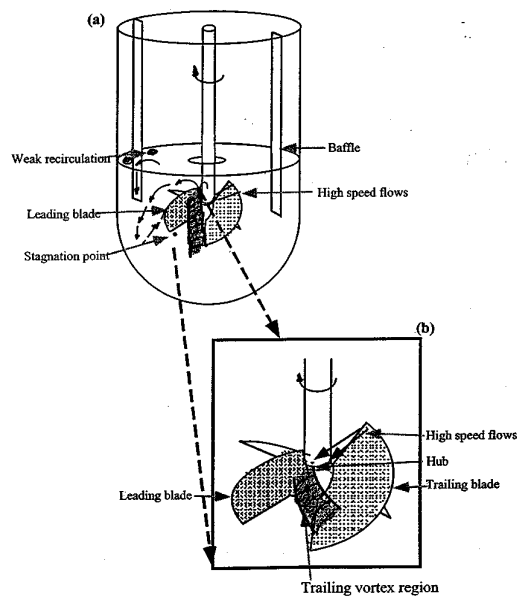


Figure 4. Schematic of the impeller flow in the case of the 20 L baffled medium-scale vessel operated at 45 rpm. (a) The overall circulation and the trailing vortex region coming off the region between the trailing tip of the leading blade and the impeller hub. (b) Magnified view (head-on front view) of the impeller stream.

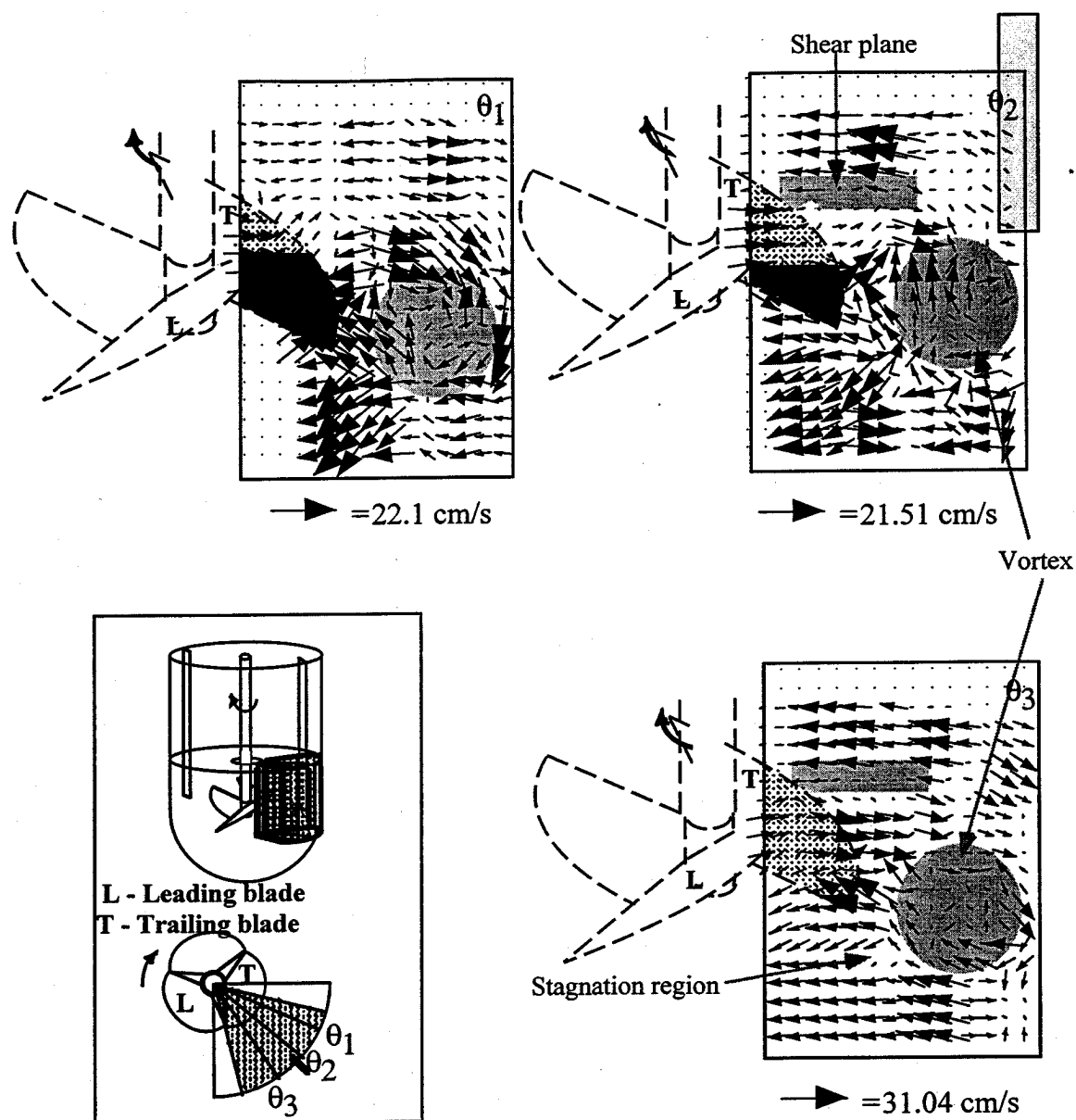


Figure 5. Mean velocity projections (V_r - V_z) in three r - z planes at $\theta_1 = 54^\circ$, $\theta_2 = 36^\circ$ and $\theta_3 = 18^\circ$ behind the trailing tip of the leading blade of the 20 L baffled medium-scale reactor agitated at 72 rpm. Reference plot shows the 20 L reactor in 3-D perspective and the location of the interpolation planes. Arrow below each of the impeller velocity projection shows the reference velocity in cm/sec. Vortex planes and shear planes are shown using shaded regions.

ular grid (for a discussion of the calculation of velocity gradients and energy parameters see Venkat *et al.*, 1996). After ensemble averaging a simple interpolation scheme was used to arrive at velocity gradients as

well as velocity planes useful for necessary graphical representation.

Table 2. Overall summary of the reactor experiments' results. The three reactors studied: 250 ml spinner, 3 L bench-scale, and 20 L medium-scale, are compared in terms of the flow structures and the mean velocity field data

Characteristic	Spinner	3 Liter bench scale	20 L medium scale
Impeller	Cylindrical stirrer (paddle)	45 ° inclined impeller (three blades)	45 ° inclined impeller (three blades)
Reynolds Number	$0.7-1.6 \times 10^4$	$0.8-2.0 \times 10^4$	$2.5-4.2 \times 10^4$
Pumping/general flow	Tangential flow	Axial up-pumping	Axial up-pumping
Vortex systems	Dual vortex from the top and the bottom of the impeller; intensity not very high	Very weak vortex flow from the trailing edge of the impeller blade; not well observed	Very well formed vortex system from the trailing edge; relatively stationary in location; continuous
Regions of high velocity gradients	Trailing vortex region; converging flow region around the impeller shaft due to formation of surface vortex	Chaotic and high speed flow in the impeller stream flowing towards stagnation region below the impeller	Impeller stream with high speed flows; trailing vortex with high shear rates

Results and discussion

General flow characteristics in the three vessels are represented in the form of schematic sketches (or cartoons). The sketches were made after careful examination of hundreds of frames of pictorial mean velocity field results obtained from the 3-D PTV experiments. The mean velocity-field results that follow the flow structures' section are some of the key results obtained. They provide the reader with methodology used by the authors to arrive at flow structures.

General flow structures

Spinner scale experiments

Figure 2 illustrates the main flow structures resulting from the paddle impeller used in spinner vessels. The impeller has sharp edges and produces flow slightly similar to a flat bladed turbine. The impeller diameter (5.6 cm) is very near the vessel diameter (7.8 cm) and the flow induced by the impeller is predominantly tangential. There is a trailing vortex region made up of a pair of vortices that come off the impeller tip. At high

agitation rates there is a strong flow that converges to the center of the vessel as a consequence of the free surface vortex. The vessel geometry (dimple at the bottom for easy lift-off of microcarriers) also results in a local region of high speed converging flow below the impeller.

Bench-scale and medium-scale experiments

Figure 3 shows a schematic of the flow in the 3 L bench-scale reactor. The predominant flow produced is high speed flow over the top of the blade and low speed flow below the blade. The trailing edge of the leading blade (refer to Figure 3 for blade nomenclature) leads to a small vortex that does not develop fully. Flow is also highly irregular in the impeller region. Sweeping blade with its sharp edges results in shear planes and regions with high fluid deformation (due to non-uniformity and gradients).

The medium-scale agitator (20 L), on the other hand, produces flow more structured than that in the bench-scale. Figure 4 illustrates main flow patterns produced by the impeller in the medium-scale vessel. Dominating flow system is a trailing vortex system

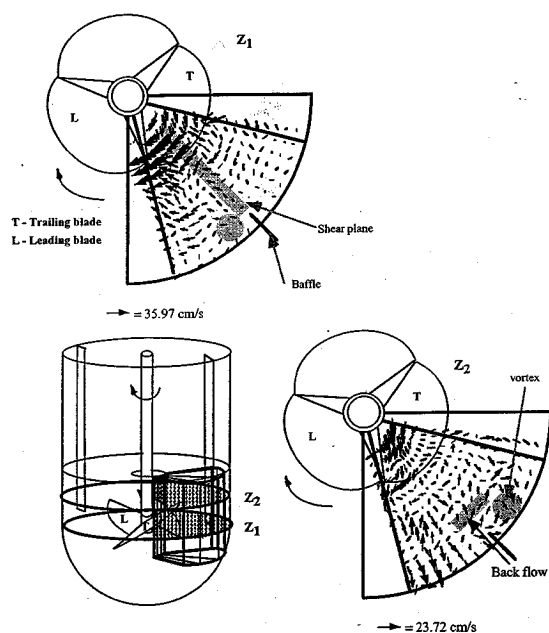


Figure 6. Mean velocity projections (V_r - V_θ) in two r - θ planes at $Z_1 = 6.22$ cm, and, $Z_2 = 10.37$ cm from the bottom of the vessel in the region behind the trailing tip of the leading blade of the 20 L medium-scale baffled reactor agitated at 45 rpm. Reference plot shows the 20 L medium-scale reactor in 3-D perspective and the location of the interpolation planes. Arrow below each of the impeller velocity projection shows the reference velocity in cm/sec. Vortex regions and shear planes are shown using shaded regions. The figure shows the effect of baffles.

behind the blades of the impeller that originates close to the impeller hub. Fluid enters the trailing vortex system due to convection resulting from up-pumping action of the impeller. The high speed above the trailing tip supplies energy to the trailing vortex system. There is also a small stagnation region below the impeller. The baffles located in the vessel do not affect the trailing vortex path or intensity because the vortex is located well below the baffles. The baffles mainly redirect the flow from radial to axial. Weak re-circulation regions were also formed behind the baffles.

Mean velocity field results

Two perspectives have been selected for display: r - θ (top views) and r - z planes. Each figure displays velocity fields at a particular impeller location and includes three 2-D slices at specified planes. The blades of the impeller have been labeled as **L** and **T** indicating *leading blade* and *trailing blade* respectively. Due to limitations on length of the paper, only key results from

the 20 L study are presented here. Other results have been presented elsewhere (Venkat, 1995).

Figure 5 represents flow behind the leading blade of the impeller. As can be seen in the Θ_3 plane, the predominant flow structure behind the blade is a well defined vortex. The trailing vortex system is fed by fluid from behind the blade convecting downwards towards the stagnation region. Flow close to the impeller tip is highly chaotic (very anisotropic, no preferred directionality to flow). This is clear in all the three planes shown in Figure 5. The trailing vortex is located below the impeller radially outward and remains relatively stationary in position. Baffles alter the direction of flow and result in a more axial flow instead of radial or tangential. They also produce wake regions made up of small recirculation regions in front of and behind the baffle. Figure 6 shows the top view (r - θ) and illustrates the effect of baffles.

Conclusions

Table 2 presents an overall summary of the hydrodynamic comparison studies performed in the three reactor vessels. It should be reiterated that the operating conditions in our studies correspond to typical scale-up conditions in industry for the microcarrier cell culture processes and were selected based on Kolmogorov eddy length criterion. There was a close geometric similarity between 3 L and 20 L reactors. But, based on the above comparison, it is clear that flow structures in the three vessels are very different from each other and the energy transfer mechanisms in the three vessels also vary significantly. It is clear that near geometric scale-up does not necessarily result in scale-up of flow structures. Based on other literature studies that have concentrated on characterization of turbulent flow structures, the ratios of the intensity of turbulent energy dissipated to the total turbulent energy content were measured to be much higher in the structures compared to the rest of the mixing tank. Therefore, in shear sensitive cultures, the flow structures can be expected to be regions where highest probability of damage due to hydrodynamic shear exists.

In future papers on the same subject, the reactors will be characterized in terms of three 'local' energy/characteristic parameters and distribution of energy in relation to flow structures further explored. 'Local' intensity of these parameters will be discussed as a function of vessel volume. By doing this, quantita-

tive results as to how the concentration of high energy regions varies from reactor can be presented.

Acknowledgements

The authors express their gratitude to Dr. Robert S. Brodkey and Dr. Yann G. Guezennec for their insight and use of PTV algorithm (YGG). Authors would also like to thank Mr. Sean Cole and Dr. Subhash Karkare, Amgen, Thousand Oaks, CA for their constant help through out this project. The research was partially supported by Amgen, Thousand Oaks, CA and the National Science Foundation, Grant # BCS 9258004.

References

- Adrian RJ (1991). Particle imaging techniques for experimental fluid mechanics. *Ann. Rev. Fluid Mech.* 185: 261–304.
- Aunins JG, Woodson Jr. BA, Hale TK and Wang DIC (1989). Effect of paddle impeller geometry on power input and mass transfer in small scale animal cell culture vessel. *Biotechnol Bioeng* 34: 1127–1132.
- Aunins JG, Glazomitsky K and Buckland BS (1993). Cell culture reactor design: known and unknown, pp. 175–190. In: Nienow AW (ed.), 3rd International Conference on Bioreactor and Bioprocess Fluid Dynamics, BHR Group Conference Series, Publication No. 5, MEP, London.
- Cherry RS and Papoutsakis ET (1986). Hydrodynamic effects in cells in agitated tissue culture reactors. *Bioproc Eng.* 1: 29–41.
- Cherry RS and Papoutsakis ET (1990). Understanding and controlling fluid mechanical injury of animal cells in bioreactors. *Animal Cell Biotechnology* 4: 71–121.
- Croughan MS, Hamel JF and Wang DIC (1987) Hydrodynamic effects on animal cells grown in microcarrier culture. *Biotechnol Bioeng* 29: 130–141.
- Guezennec YG, Brodkey RS, Trigui N and Kent JC (1994). Algorithms for fully automated three-dimensional particle tracking velocimetry. *Exp. Fluids* 17: 209–219.
- Oldshue JY (1983). *Fluid Mixing Technology*. McGraw-Hill, New York. p. 89.
- Papoutsakis ET (1991). Fluid-mechanical damage of animal cells in bioreactors. *Trends Biotech.* 9: 427–437.
- Smith GW, Tavlarides LL and Placek J (1990). Turbulent flow in stirred tanks: Scale-up computations for vessel hydrodynamics. *Chem. Eng. Comm.* 93: 49–81.
- Stoots CM and Calabrese RV (1995). Mean velocity relative to a Rushton turbine blade. *AIChE J.* 41: 1–11.
- Tennekes H and Lumley JL (1972). *First course in turbulence*. MIT Press, Cambridge, MA.
- Venkat RV, Brodkey RS, Guezennec YG and Chalmers JJ (1993). Experimental determination of local hydrodynamic information in microcarrier culture spinner vessels, pp. 483–501. In: Nienow AW (ed.), 3rd International Conference on Bioreactor and Bioprocess Fluid Dynamics, BHR Group Conference Series, Publication No. 5, MEP, London.
- Venkat RV (1995). Study of hydrodynamics due to turbulent mixing in animal cell microcarrier bioreactors. Doctoral dissertation, Department of Chemical Engineering, The Ohio State University, Columbus, Ohio.
- Venkat RV, Stock RL and Chalmers JJ (1996). Study of hydrodynamics in microcarrier culture spinner vessels – a particle tracking velocimetry approach. *Biotechnol. Bioeng.* 49: 456–466.

Address for correspondence: J. J. Chalmers, 140 W. 19th Avenue, Department of Chemical Engineering, The Ohio State University, Columbus, OH 43210–1180, USA